RSC Advances

PAPER

View Article Online
View Journal | View Issue

Check for updates

Cite this: *RSC Adv.*, 2019, **9**, 39435

The nature of G···E–Y σ(3c–4e) in *o*-$Me_nGCH_2C_6H_4EY$ (Me_nG = Me_2N and MeE; E = O, S, Se and Te; Y = F, Cl, Br, EMe and Me) with contributions from CT and compliance constants in noncovalent G···E interactions†

Satoko Hayashi,*[a] Taro Nishide,[a] Waro Nakanishi,*[a] Luca Sancineto[bc] and Claudio Santi*[c]

The intrinsic dynamic and static nature of G–*–E–*–Y σ(3c–4e) interactions was elucidated with the quantum theory of atoms in molecules dual functional analysis (QTAIM-DFA), employing *o*-$Me_nGCH_2C_6H_4EY$ (Me_nG = Me_2N and MeE; E = O, S, Se and Te; Y = F, Cl, Br, I, EMe and Me). Asterisks (*) are employed to emphasize the existence of bond critical points (BCPs) on the bond paths (BPs), corresponding to the interactions in question. Data from the fully optimized structure correspond to the static nature of interactions. The dynamic nature is called the intrinsic dynamic nature if the perturbed structures are generated using the coordinates derived from the compliance constants. Basis sets of the Sapporo-TZP type with diffusion functions are employed for the heteroatoms at the MP2 level. The noncovalent G–*–E interactions in GEY σ(3c–4e) are predicted to demonstrate van der Waals bonding to CT-TBP (trigonal bipyramidal adduct formation through charge transfer) nature, while the E–*–Y bonds have the covalent nature. Some E–F bonds show strong ionic character when G–*–E is predicted to be stronger than E–*–Y. The contributions of the CT terms to the G–*–E interactions, evaluated with NBO, are discussed in relation to the predicted nature. The *E*(2) values based on NBO are strongly correlated to the compliance constants for the G–*–E interactions if suitably treated separately.

Received 1st November 2019
Accepted 20th November 2019

DOI: 10.1039/c9ra09022c

rsc.li/rsc-advances

Open Access Article. Published on 29 November 2019. Downloaded on 7/18/2024 8:24:35 PM.
This article is licensed under a Creative Commons Attribution-NonCommercial 3.0 Unported Licence.

Introduction

Weak interactions in chemistry, such as van der Waals (vdW), hydrogen bonds (HB) and charge transfer (CT) interactions, determine the fine details of the structure of molecules and create the functionalities of materials; strong interactions, such as classical chemical bonds, construct the framework of molecules. Weak interactions play a crucial role in the modulation of biological properties of selenium and sulfur containing compounds, driving their activity towards a protective antioxidant effect or a toxic pro-oxidant effect.[1] Three-centre four-electron interactions of the σ-type (σ(3c–4e)) are typical in cases of such weak interactions, which determine fine details of these structures.[2–4] The concept of σ(3c–4e) was first proposed by Musher, Pimentel, and Rundle.[2a–2d] It was developed through the preparation and characterization of such compounds and theoretical investigations mainly by Martin,[2e] Akiba,[4a] Schleyer[3e] and others.[3a–3d,4b,4c] Lots of sulfuranes of the symmetric and unsymmetric types were prepared by Martin and coworkers.[2e] They clarified the behaviour of unsymmetric σ(3c–4e) in sulfuranes, through the careful investigations of the interactions.[2e]

The CT interactions between nonbonded orbitals of G (n(G)) and the σ*-orbitals of E–Y (σ*(E–Y)) are also typically described as G···E–Y σ(3c–4e). The interactions should be denoted by unsymmetric GEY σ(3c–4e), since they must be (very) unsymmetric. Nevertheless, they will be described as GEY σ(3c–4e), here, for the simplification of notation. Scheme 1 illustrates the structures of the target species in this work **1–5** and the related ones **I** and **6**, together with the approximate MO model for GEY σ(3c–4e) and the simplified interaction model for GEY σ(3c–4e). While the models may evoke the image of symmetric GEY σ(3c–4e), the contributions from the p-AOs on GEY σ(3c–4e) will change depending on the unsymmetric nature of GEY σ(3c–4e). The system will be energetically stabilized most effectively through GEY σ(3c–4e) when the three GEY atoms align linearly,

[a]*Faculty of Systems Engineering, Wakayama University, 930 Sakaedani, Wakayama 640-8510, Japan. E-mail: hayashi3@sys.wakayama-u.ac.jp; nakanisi@sys.wakayama-u.ac.jp; Tel: +81 73 457 8252*

[b]*Organic Chemistry Section, Center of Molecular and Macromolecular Studies, Polish Academy of Sciences, Sienkiewicza 112, 90-363, Lódz, Poland*

[c]*Dipartimento di Chimica e Tecnologia del Farmaco, Università degli Studi di Perugia, Via del Liceo 1, 06123 Perugia, Italy. E-mail: claudio.santi@unipg.it; Tel: +39 075 5855102*

† Electronic supplementary information (ESI) available: QTAIM-DFA approach, computational data, and the fully optimized structures given by Cartesian coordinates, together with total energies of **1–5**. See DOI: 10.1039/c9ra09022c

Open Access Article. Published on 29 November 2019. Downloaded on 7/18/2024 8:24:35 PM.
This article is licensed under a Creative Commons Attribution-NonCommercial 3.0 Unported Licence.

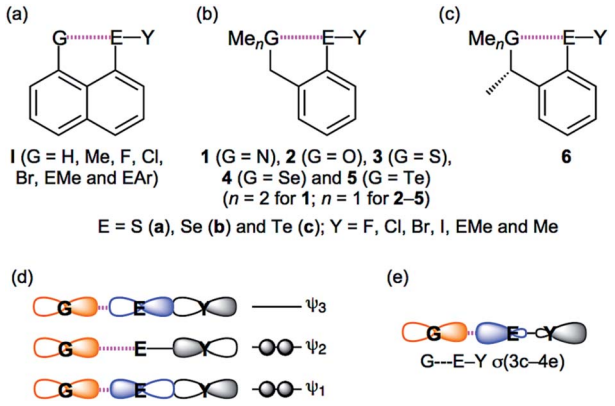

Scheme 1 Structures of **I** (a) and **1–6** (b and c), together with the approximate MO model of GEY σ(3c–4e) (d) and the simplified interaction model for GEY σ(3c–4e) (e).

allowing the orbital between n(G) and σ*(E–Y) to overlap most effectively. As a result, the formation of GEY σ(3c–4e) makes the three atoms align linearly. Such linear alignment of the three atoms is typically observed in conventional HBs of the shared proton interaction type (cv-HBs: B···H–X). The unsymmetric B···H–X σ(3c–4e) is formed through the reaction between electron donor B and acceptor H–X. Energies in the formation of cv-HBs are typically 10–40 kJ mol^{-1} for the neutral form,[5–8] although HBs spread over a wide range from vdW to covalent bonds. The nature of BHX σ(3c–4e) have been reported recently.[9,10]

There has been much interest in the weak interactions of GEY σ(3c–4e), rather than BHX σ(3c–4e), in cv-HBs. The chemistry originating from GEY σ(3c–4e) in the naphthalene 1,8-positions of 8-G–$C_{10}H_6$–EY-1 (**I**) has been studied thoroughly by Wakayama group.[11] The linear alignment of the three GEY atoms was called "G-dependence", especially for Y = C, and the donor ability for G = F is demonstrated. The nature of G···E–Y in **I** is clarified, which is discussed elsewhere.[11a,11c,11d,11f,11h] The benzyl type species of *o*-$MeGCH_2C_6H_4EY$ (**1–5**) are also important candidates to investigate the chemistry originating from GEY σ(3c–4e). Structure analysis, spectroscopic analysis and reactivity in asymmetric synthesis for GEY σ(3c–4e) were investigated by employing the methyl derivatives of **1–5** (**6**) in Perugia.[12] Surprisingly, short Se···S distances were observed in **6** (2.344(2) Å for (G, E, Y) = (S, Se, Cl) and 2.497(7) Å for (S, Se, Br)). Iwaoka and Tomoda also investigated the GEY σ(3c–4e) type interactions, employing **1–5** or similar.[13] They reported the negative values of the total electron energy densities at bond critical points ($H_b(r_c)$) for O···Se in **2** (EY = SeCl and SeBr), benzyl alcohols and 2-formyl derivatives. As shown in Scheme 1, GEY σ(3c–4e) in **1–5** seem closely related to X–H···F–Y investigated by Espinosa and co-workers,[14] although some of the latter interactions should be analyzed by the σ(4c–6e) model.

What is the behaviour of GEY σ(3c–4e)? The nature of the noncovalent G···E interactions and the (covalent) E–Y bonds in G···E–Y σ(3c–4e) is elucidated by employing **1–5**, rather than **I**, where the noncovalent G···E interactions are synonymous with the closed shell (CS) interactions, in this work. Indeed, stronger G···E interactions are expected to be detected in **I**, but the framework around the naphthalene 1,8-positions in **I** seems too rigid to detect the delicate behaviour of the GEY interactions. Instead, the framework around GEY σ(3c–4e) in **1–5** seems suitably flexible, which would be more advantageous for elucidating the fine details of the GEY σ(3c–4e) nature originating from the delicate properties of G, E and Y, relative to the case of **I**.[15]

How can the nature of GEY σ(3c–4e) be clarified? The quantum theory of atoms in molecules (QTAIM) approach, introduced by Bader,[16,17] enables us to analyze the nature of chemical bonds and interactions.[18–22] A bond critical point (BCP, *) is an important concept in QTAIM approach in which $\rho(r)$ (charge density) reaches a minimum along the interatomic (bond) path and a maximum on the interatomic surface separating the atomic basins. The $\rho(r)$ at the BCP is described by $\rho_b(r_c)$, as well as other QTAIM functions, such as $H_b(r_c)$, potential energy densities $V_b(r_c)$ and kinetic energy densities $G_b(r_c)$. A chemical bond or interaction between atoms A and B is denoted by A–B, which corresponds to the bond path (BP) in QTAIM. We will use A–*–B for BP, where the asterisk emphasizes the existence of a BCP in A–B.[16,17,23] Eqn (1), (2) and (2′) represent the relations between $G_b(r_c)$, $V_b(r_c)$, $H_b(r_c)$ and $\nabla^2\rho_b(r_c)$. $H_b(r_c)$ must be negative when $\nabla^2\rho_b(r_c) < 0$ since $V_b(r_c)$ are negative at all BCPs (*cf.*: eqn (2)).

$$H_b(r_c) = G_b(r_c) + V_b(r_c) \quad (1)$$

$$(\hbar^2/8m)\nabla^2\rho_b(r_c) = H_b(r_c) - V_b(r_c)/2 \quad (2)$$

$$= G_b(r_c) + V_b(r_c)/2 \quad (2')$$

Interactions are classified by the signs of $\nabla^2\rho_b(r_c)$ and $H_b(r_c)$. They are called shard shell (SS) interactions for those with $\nabla^2\rho_b(r_c) < 0$ (and $H_b(r_c) < 0$) and CS interactions for those with $\nabla^2\rho_b(r_c) > 0$.[14] The CS interactions are especially called pure CS (p-CS) interactions when $H_b(r_c) > 0$ with $\nabla^2\rho_b(r_c) > 0$. We call such interactions regular CS (r-CS) interactions that have the QTAIM values of $H_b(r_c) < 0$ and $\nabla^2\rho_b(r_c) > 0$, which distinguish the interactions clearly from the p-CS interactions. The signs of $\nabla^2\rho_b(r_c)$ can be replaced by those of $H_b(r_c) - V_b(r_c)/2$ in the discussion, since $(\hbar^2/8m)\nabla^2\rho_b(r_c) = H_b(r_c) - V_b(r_c)/2$ (see, eqn (2)). Details are explained later, again.

Recently, the QTAIM dual functional analysis (QTAIM-DFA) was formulated based on the QTAIM approach, allowing experimental chemists to analyse their own chemical bond and interaction results based on their own expectations.[24–28] In QTAIM-DFA, we proposed to use the signs of the first derivatives of $H_b(r_c) - V_b(r_c)/2$ and $H_b(r_c)((H_b(r_c) - V_b(r_c)/2)/dr$ and $H_b(r_c)/dr$, respectively), in addition to the signs of $H_b(r_c) - V_b(r_c)/2$ and $H_b(r_c)$, to classify (and characterize) the interactions. $H_b(r_c)$ are plotted *versus* $H_b(r_c) - V_b(r_c)/2$ ($= (\hbar^2/8m)\nabla^2\rho_b(r_c)$) (*cf.*: eqn (2)) at BCPs in QTAIM-DFA. Data from the fully optimized structures are analysed using the polar coordinate (R, θ) representation,[29] which correspond to the static natures of the interactions.[24a,25–28] Data from the perturbed structures around the fully optimized structures are employed, in addition to those

 This journal is © The Royal Society of Chemistry 2019

Open Access Article. Published on 29 November 2019. Downloaded on 7/18/2024 8:24:35 PM.
This article is licensed under a Creative Commons Attribution-NonCommercial 3.0 Unported Licence.

from the fully optimized structures, in our treatment. Each interaction plot, which contains data from both the perturbed and fully optimized structures, includes a specific curve that provides important information about the interaction. This plot is expressed by (θ_p, κ_p), where θ_p corresponds to the tangent line of the plot and κ_p is the curvature. The dynamic nature of interactions was proposed based on (θ_p, κ_p).[29] We call (R, θ) and (θ_p, κ_p) the QTAIM-DFA parameters, which are illustrated in Fig. 3 and exemplified by the intramolecular S–*–SF interaction in **3a**.

It is necessary to establish a reliable method to generate the perturbed structures for the effective analysis with QTAIM-DFA. We recently proposed a highly reliable method to generate the perturbed structures for QTAIM-DFA.[30] The method is called CIV and employs the coordinates derived from the compliance constants C_{ii} for the internal vibrations. Eqn (3) defines C_{ij}, as the partial second derivatives of the potential energy due to an external force, where i and j refer to internal coordinates, and the force constants f_i and f_j correspond to i and j, respectively. While the off-diagonal elements C_{ij} ($i \neq j$) in eqn (3) correspond to the compliance coupling constants, the diagonal elements C_{ii} represent the compliance constants for an internal coordinate i. The C_{ii} values and coordinates corresponding to C_{ii} were calculated using the Compliance 3.0.2 program[31] released by Grunenberg and Brandhorst.[32] The dynamic nature of interactions based on the perturbed structures with CIV is described as the "intrinsic dynamic nature of interactions," as the coordinates are invariant to the choice of the coordinate system.

$$C_{ij} = \partial^2 E/\partial f_i \partial f_j \quad (3)$$

QTAIM-DFA is applied to standard interactions, and rough criteria to distinguish the interaction in question from others are obtained. The applications of CIV to the CS interactions are substantially more effective than those to the SS interactions in QTAIM-DFA.[30] QTAIM-DFA has excellent potential for evaluating, classifying, characterizing and understanding weak to strong interactions according to a unified form.[24a,25–28,30] The basis sets and levels for the calculations must also be important when the calculated nature is discussed in relation to the observed results.[33] Therefore, higher basis set systems are used for the calculations. QTAIM-DFA and the criteria are explained in the ESI using Schemes S1–S3, Fig. S1, S2, Table S1 and eqn (S1)–(S7).† The basic concept of the QTAIM approach is also explained.

The negative values of $H_b(r_c)$, reported for O···Se in **2** (EY = SeCl and SeBr), predict the covalent contribution in these interactions, which correspond to the static nature, although $H_b(r_c)$ for O···Se in **2** (EY = SeBr) is positive in our calculations. The nature of the interactions will be discussed latter again. However, the dynamic nature is to be elucidated for GEY σ(3c–4e) for better understanding of the interactions. QTAIM-DFA employing the perturbed structures generated with CIV is well-suited to elucidate the intrinsic dynamic and static nature of GEY σ(3c–4e) of **1–5**. Herein, we present the results of calculations on the intrinsic dynamic and static nature of the interactions. The interactions are classified and characterized by employing the criteria as a reference. NBO analysis is applied to the interactions in question in **1–5**. The nature of the interactions will also be discussed in relation to the interaction energies calculated with NBO ($E(2)$) and the structural features. A proportional relationship is detected between $E(2)$ and C_{ii}.

Methodological details in calculations

Gaussian 09 programs[34] were employed for the calculations, containing the NBO analysis.[35] The basis sets of the (6211/311/21/2 + 1s1p), (63211/6111/31/2 + 1s1p1d1f), (743211/74111/721/2 + 1s1p1d1f) and (7433111/743111/7411/2 + 1s1p1d1f) types were employed for (O, F), (S, Cl), (Se, Br) and (Te, I), respectively, as implemented from the Sapporo Basis Set Factory,[36] with the 6-311G(d) basis set for C and H. The basis set system is called A (BSS-A). The Møller–Plesset second order energy correlation (MP2) level[37] was applied to the calculations (MP2/BSS-A). The results of the frequency analysis were used to obtain the compliance constants (C_{ij}) and the coordinates corresponding to C_{ij}.[31] The optimizations were not corrected with the BSSE method.

Eqn (4) explains the method to generate the perturbed structures with CIV.[30] A i-th perturbed structure in question ($\mathbf{S}_{iw}$) is generated by the addition of the coordinates corresponding to C_{ii} in eqn (3) (C_i) to the standard orientation of a fully optimized structure ($\mathbf{S}_o$) in the matrix representation. The coefficient g_{iw} in eqn (4) controls the structural difference between S_{iw} and S_o:[38] g_{iw} is determined to satisfy eqn (5) for r. The C_i values of five digits are used to predict S_{iw}.

$$\mathbf{S}_{iw} = \mathbf{S}_o + g_{iw}C_i \quad (4)$$

$$r = r_o + wa_o \ (w = (0), \pm 0.025 \text{ and } \pm 0.05;\ a_o = 0.52918 \text{ Å}) \quad (5)$$

$$y = c_o + c_1 x + c_2 x^2 + c_3 x^3$$
(R_c^2: square of correlation coefficient.) (6)

QTAIM functions were calculated with the same method as the optimizations at the MP2 level, unless otherwise noted. The calculated values were analysed with the AIM2000 [39] and AIMAll[40] programs. $H_b(r_c)$ are plotted *versus* $H_b(r_c) - V_b(r_c)/2$ for data of five points of $w = 0$, ± 0.05 and ± 0.1 in eqn (5) in QTAIM-DFA. Each plot is analysed using a regression curve of the cubic function, shown in eqn (6), where (x, y) = ($H_b(r_c) - V_b(r_c)/2$, $H_b(r_c)$) ($R_c^2 > 0.99999$ is typical).[27]

Results and discussion

Optimizations of species, 1–5

Selected structural parameters, r(G, E), r(E, Y) and ∠GEY, of **1a**, **1b**, **2a**, **2b**, **3a**, **3b**, **4a**, **4b** and **5c** (**1–5**), optimized with MP2/BSS-A, are collected in Table S2 of the ESI,† with the Δr(G, E) and Δr(E, Y) values. Eqn (7) defines the Δr(G, E) values as the differences from the sum of the van der Waals radii of G and E, while eqn (8) produces the Δr(E, Y) values as the differences from the sum of the covalent radii of E and Y.

$$\Delta r(\text{G, E}) = r(\text{G, E}) - (r_{vdW}(\text{G}) + r_{vdW}(\text{E})) \quad (7)$$

Open Access Article. Published on 29 November 2019. Downloaded on 7/18/2024 8:24:35 PM.
This article is licensed under a Creative Commons Attribution-NonCommercial 3.0 Unported Licence.

$$\Delta r(\mathrm{E,\ Y}) = r(\mathrm{E,\ Y}) - (r_{co}(\mathrm{E}) + r_{co}(\mathrm{Y})) \quad (8)$$

Fig. 1 shows the plot of Δr(G, E) *versus* Y for **1–5**. The Δr(G, E) values change depending on G, E and Y, as shown in Fig. 1. The Δr(E, Y) values are plotted *versus* Δr(G, E), although that of **1** is tentative. The plot is shown in Fig. S5 of the ESI.† The Δr(E, Y) values are expected to change in a manner that is inversely proportional to Δr(G, E). The inverse proportionality between Δr(G, E) and Δr(E, Y) is well recognized if the plots are analysed separately by **2** and **3–5**, with the exceptions of Y = F and EMe in G···E–Y of **2–5**. The exceptions correlate well, although the data for O···E–F (E = S and Se) and Te···Te–F are neglected. Fortunately, the neglected three data points also showed good correlation. As a result, the plot is finally analysed as five correlations.

The results can be explained by assuming that the total covalency of the central atom E in GEY σ(3c–4e) is almost constant when G and Y are changed. A valence atomic p-orbital of E, in the linear GEY direction, is employed to connect G and Y to E to form GEY σ(3c–4e) in the species (see Scheme 1c). Specifically, E–Y will be weaker if G···E becomes stronger in GEY σ(3c–4e). The ∠GEY values must be 180° or larger than 150° for G···E–Y interactions to be analysed as linear σ(3c–4e), where ∠GEY of 150° is the tentative value, which we proposed as a lower limit for the linear interactions. The ∠GEY values drop in the range of 165° to 175°, which satisfy the above explanation.

Before a discussion of the nature of GEY σ(3c–4e), it is necessary to examine the molecular graphs with contour plots.

Molecular graphs with contour plots for 1–5

The molecular graphs with the contour plots are drawn for **1–5**. Fig. 2 illustrates the contour exemplified by 4b with Y = F, Cl, Br, I, SeMe and Me. All BCPs are clearly detected, containing those for the noncovalent G–*–E interactions and the E–*–Y bonds. The BCPs are well located at the (three-dimensional) saddle points of $\rho(r)$. Similar results are obtained for **1–5**, other than **4b** in Fig. 2, although the BP with BCP corresponding to the Se···SC_{Me} in **4a** is not detected.

BPs, corresponding to the noncovalent G···E interactions, appear straight, as shown in Fig. 2. To examine the linearity of the noncovalent interactions further, the lengths of the BPs (r_{BP}) in question and the corresponding straight-line distances (R_{SL}) are calculated for G···E in **1–5**. The values calculated with MP2/BSS-A are collected in Table S3 of the ESI,† with the differences between the two ($\Delta r_{BP} = r_{BP} - R_{SL}$). The magnitudes of Δr_{BP} are 0.001–0.022 Å for the BPs. Consequently, the noncovalent G···E interactions in **1–5** can be approximated as straight.

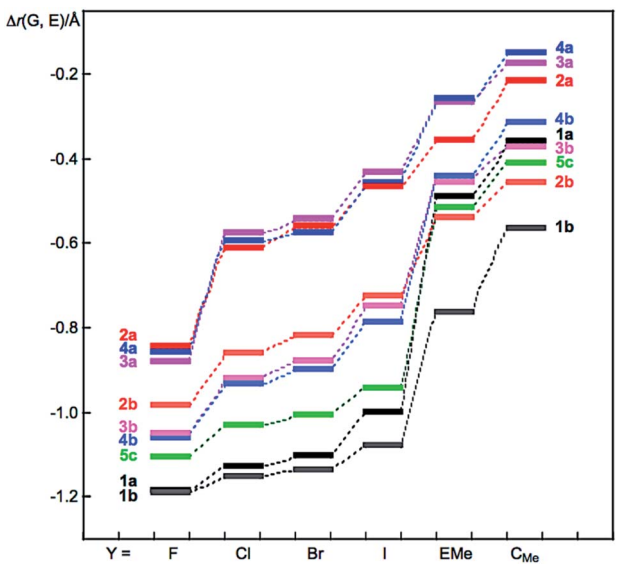

Fig. 1 Plots of Δr(G, E) *versus* Y for **1–5**, evaluated with MP2/BSS-A.

QTAIM-DFA treatment of the G···E and E–Y interactions in 1–5

QTAIM functions of $\rho_b(r_c)$, $H_b(r_c) - V_b(r_c)/2$ and $H_b(r_c)$ are calculated for the noncovalent G···E interactions and the E–Y bonds at BCPs in noncovalent G···E interactions, while those for the E–Y bonds are collected in Table S4 of the ESI.† Fig. 3 shows the plots of $H_b(r_c)$ **1–5** with MP2/BSS-A. Table 1 summarizes the values for the *versus* $H_b(r_c) - V_b(r_c)/2$ for the data in Table 1 and those from the perturbed structures, generated with CIV, as shown for G···E in **3a**, **4b** and **5c**. Fig. 3 shows that the noncovalent G···E interactions become stronger in the order of G···E = S···S < Se···Se < Te···Te. The $H_b(r_c)$ values are negative for all Te–*–Te in **5c**, indicating that the interactions contain covalent nature appeared in the regular CS region. The QTAIM-DFA parameters of (R, θ) and (θ_p, κ_p) for G–*–E in GEY σ(3c–4e) were obtained for **3a**, **4b** and **5c** by analysing the plots in Fig. 3, according to eqn (S1)–(S6) of the ESI.† The values for G–*–E in **1–5**, but not **3a**, **4b** and **5c**, were similarly obtained, with the exception of Se···SC_{Me} in **4a**. Table 1 shows the values for G–*–E in **1–5**. The (R, θ) and (θ_p, κ_p) values for E–*–Y are similarly calculated, and these values are presented in Table S4 of the ESI.† The C_{ii} values, corresponding to CIV employed to generate the perturbed structures, are also given in the tables. The noncovalent G···E interactions and the E–Y bonds of GEY σ(3c–4e) in **1–5** are classified and characterized based on the (R, θ, θ_p) values, employing the standard values as a reference. The results evaluated with MP2/BSS-A are summarized in Table 2.

Nature of the G···E and E–Y interactions in 1–5

The criteria to classify the interactions in question is formulated based on the signs of $H_b(r_c) - V_b(r_c)/2$ and $H_b(r_c)$, similarly to those by Espinosa and coworkers.[14,41] In this classification, we employ regular CS interactions for those with $0 < H_b(r_c) - V_b(r_c)/2$ and $0 > H_b(r_c)$ to distinguish the CS interactions of the region from pure CS interactions of $0 < H_b(r_c) - V_b(r_c)/2$ and $0 < H_b(r_c)$. The criteria also characterize the interactions in question by using the signs of $d(H_b(r_c) - V_b(r_c)/2)/dr$ and $dH_b(r_c)/dr$, although $dH_b(r_c)/(H_b(r_c) - V_b(r_c)/2)$ is employed in QTAIM-DFA, as aforementioned. Interactions in question will be classified and characterized by θ and θ_p, respectively, after the treatment of the interactions in question with QTAIM-DFA.

It is instructive to survey the criteria shown in Scheme S3 and Table S1 of the ESI,† before detailed discussion. The criteria tell us that $45° < \theta < 180°$ ($0 < H_b(r_c) - V_b(r_c)/2$) for the CS

This journal is © The Royal Society of Chemistry 2019

Open Access Article. Published on 29 November 2019. Downloaded on 7/18/2024 8:24:35 PM.
This article is licensed under a Creative Commons Attribution-NonCommercial 3.0 Unported Licence.

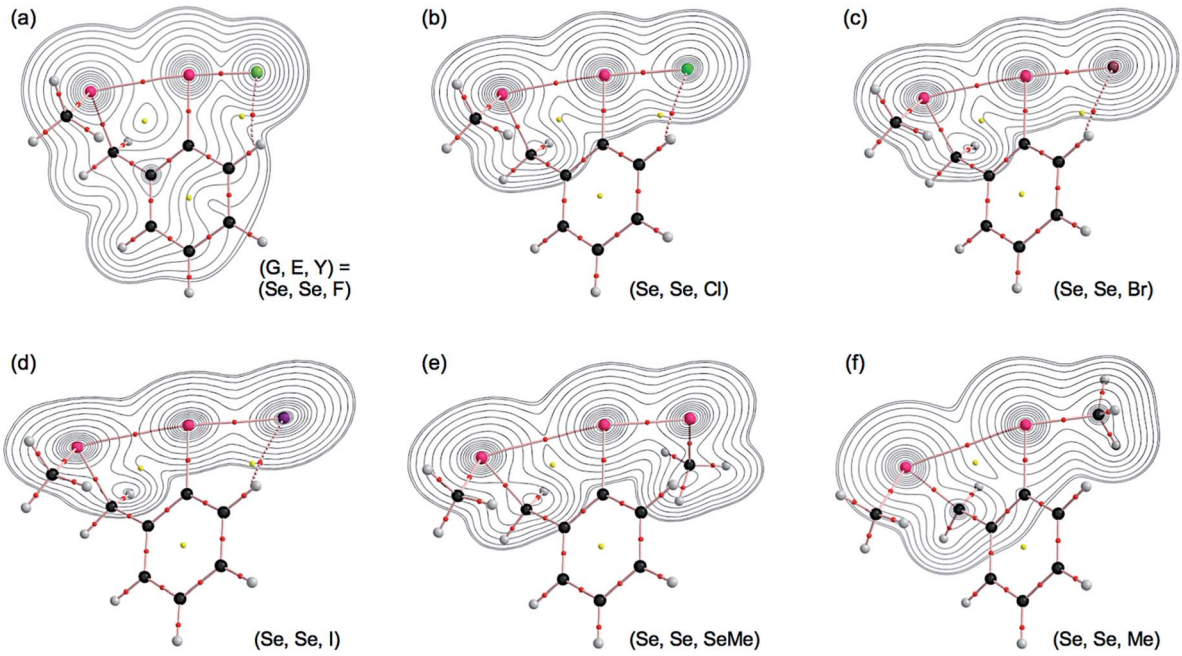

Fig. 2 Molecular graphs for **4b**, where Y = F, Cl, Br, I, SeMe and Me, ((a)–(f), respectively) calculated with MP2/BSS-A. BCPs are denoted by red dots, RCPs (ring critical points) by yellow dots and BPs by pink lines. Carbon, hydrogen, selenium, fluorine, chlorine, bromine and iodine atoms are shown in black, grey, pink, light green, green, purple and dark purple, respectively. Contour plots are drawn on the planes containing GEY σ(3c–4e). The contours (ea_o^{-3}) are at 2^l ($l = \pm 8, \pm 7, \ldots$ and 0).

interactions and $180° < \theta < 206.6°$ ($H_b(r_c) - V_b(r_c)/2 < 0$) for the SS interactions.[28] The CS interactions are sub-divided into $45° < \theta < 90°$ ($H_b(r_c) > 0$) for the pure CS (p-CS) interactions and $90° < \theta < 180°$ ($H_b(r_c) < 0$) for the regular CS (r-CS) interactions.[14,16,17,24,25] In the p-CS region of $45° < \theta < 90°$, the character of interactions will be the vdW type for $45° < \theta_p < 90°$ ($45° < \theta < 75°$), whereas it will be t-HB_{nc} (the typical hydrogen bonds type with no covalency) for $90° < \theta_p < 125°$ ($75° < \theta < 90°$), where $\theta = 75°$ and $\theta_p = 125°$ are tentatively given to satisfy $\theta_p = 90°$ and $\theta = 90°$, respectively. The CT interactions will appear in the r-CS region of $90° < \theta < 180°$. The t-HB interactions with covalency (t-HB_{wc}) appear in the range of $125° < \theta_p < 150°$ ($90° < \theta < 115°$), where (θ, θ_p) = (115°, 150°) are tentatively borderline between the nature of t-HB_{wc} and CT-MC (molecular complex formation through CT). The borderline interactions between CT-MC and CT-TBP (trigonal bipyramidal adduct formation through CT) is defined by (θ, θ_p) = (150°, 180°), where $\theta = 150°$ is tentatively given corresponding to $\theta_p = 180°$. As a result, the (θ, θ_p) values of (75°, 90°), (90°, 125°), (115°, 150°), (150°, 180°) and (180°, 190°) correspond to the borderlines between the nature of interactions for vdW/t-HB_{nc}, t-HB_{nc}/t-HB_{wc}, t-HB_{wc}/CT-MC, CT-MC/CT-TBP and CT-TBP/Cov-w (weak covalent bonds), respectively. The covalent bonds (Cov) will be strong (Cov-s) if $R > 0.15$ au, but they will be weak for $R < 0.15$ au (Cov-w). $\theta_p = 190°$ is tentatively given for $\theta = 180°$, the border for CT-TBP/Cov-w. The parameters, described in bold, are superior to the tentatively given parameters, described in plane, in the classification and/or characterization of interactions. However, the rule should be carefully applied to the E–F bonds since the values of $H_b(r_c) - V_b(r_c)/2$ and $H_b(r_c)$ will be greater for the bonds containing F.[42]

The nature of the E–*–Y bonds is discussed first. The (R, θ, θ_p) values are (0.034–0.132 au, 180.3–196.0°, 187.9–199.7°) for E = S of the S–*–Cl, S–*–Br, S–*–I, S–*–SMe and/or S–*–C_{Me} interactions with G = N, O, S and Se, except for GE–*–Y = NS–*–Br, of which (R, θ, θ_p) are (0.038 au, 176.7°, 193.9°). Therefore, the interactions of the former are typically classified as the SS interactions and characterized to be the Cov-w nature (SS/Cov-

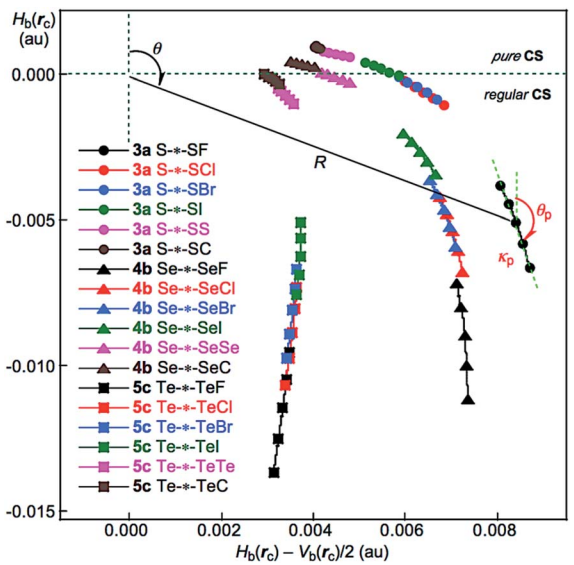

Fig. 3 Plots of $H_b(r_c)$ *versus* $H_b(r_c) - V_b(r_c)/2$ for G–*–E in GEY σ(3c–4e), as shown for **3a**, **4b** and **5c**. Perturbed structures are generated with CIV.

Open Access Article. Published on 29 November 2019. Downloaded on 7/18/2024 8:24:35 PM.
This article is licensed under a Creative Commons Attribution-NonCommercial 3.0 Unported Licence.

Table 1 The QTAIM functions, QTAIM-DFA parameters and C_{ii} values for the noncovalent G–*–E interactions in GEY σ(3c–4e) of **1a–5c** predicted with MP2/BSS-A[a]

Species: G–*–EY	$\rho_b(r_c)$ (ea_o^{-3})	$c\nabla^2\rho_b(r_c)$[b] (au)	$H_b(r_c)$ (au)	R[c] (au)	θ[d] (°)	C_{ii}[e] (Å mdyn^{-1})	θ_p[f] (°)	κ_p[g] (au^{-1})
1a: N–*–SF	0.0815	0.0094	−0.0289	0.0303	162.0	1.505	189.9	5.2
1a: N–*–SCl	0.0738	0.0108	−0.0216	0.0241	153.4	2.331	187.7	9.1
1a: N–*–SBr	0.0713	0.0112	−0.0195	0.0225	150.2	2.510	186.4	11.6
1a: N–*–SI	0.0573	0.0121	−0.0109	0.0163	132.0	5.172	179.2	23.4
1a: N–*–SSMe	0.0198	0.0074	0.0008	0.0074	84.1	8.174	106.0	117
1a: N–*–SC_{Me}	0.0152	0.006	0.0011	0.0061	79.7	7.757	96.1	76.2
1b: N–*–SeF	0.0713	0.0106	−0.0235	0.0258	155.6	1.318	182.4	3.1
1b: N–*–SeCl	0.0680	0.0107	−0.0202	0.0228	152.1	1.659	183.1	7.1
1b: N–*–SeBr	0.0662	0.0108	−0.0187	0.0216	150.0	1.763	182.6	9.9
1b: N–*–SeI	0.0597	0.0112	−0.0141	0.0180	141.5	2.244	180.5	12.8
1b: N–*–SeSeMe	0.0314	0.0098	−0.0014	0.0099	98.2	5.408	140.3	140
1b: N–*–SeC_{Me}	0.0209	0.0075	0.0006	0.0075	85.3	6.266	107.5	137
2a: O–*–SF	0.0330	0.0134	−0.0001	0.0134	90.3	5.337	124.6	132
2a: O–*–SCl	0.0212	0.0093	0.0015	0.0094	80.8	8.067	95.0	76.8
2a: O–*–SBr	0.0196	0.0086	0.0015	0.0088	79.9	8.546	92.5	68.0
2a: O–*–SI	0.0165	0.0074	0.0016	0.0075	78.1	9.674	88.2	51.4
2a: O–*–SSMe	0.0133	0.0061	0.0015	0.0063	76.5	9.033	84.9	14.2
2a: O–*–SC_{Me}	0.0120	0.0056	0.0014	0.0058	75.7	8.770	84.4	45.9
2b: O–*–SeF	0.0399	0.0146	−0.0029	0.0149	101.4	2.904	147.4	79.4
2b: O–*–SeCl	0.0320	0.0126	−0.0003	0.0126	91.1	4.307	125.9	125
2b: O–*–SeBr	0.0299	0.0119	0.0002	0.0119	88.9	4.791	119.2	127
2b: O–*–SeI	0.0250	0.0102	0.0010	0.0103	84.4	5.925	105.3	112
2b: O–*–SeSeMe	0.0176	0.0075	0.0014	0.0076	79.4	7.396	89.0	67.3
2b: O–*–SeC_{Me}	0.0149	0.0065	0.0014	0.0066	77.6	7.557	84.2	48.3
3a: S–*–SF	0.0389	0.0084	−0.0051	0.0098	121.2	7.613	167.1	68.8
3a: S–*–SCl	0.0220	0.0064	−0.0006	0.0064	95.4	9.525	133.8	162
3a: S–*–SBr	0.0210	0.0063	−0.0004	0.0063	93.9	10.027	131.4	167
3a: S–*–SI	0.0169	0.0055	0.0002	0.0055	87.9	12.043	121.5	174
3a: S–*–SSMe	0.0121	0.0045	0.0007	0.0045	81.0	9.477	109.4	30.8
3a: S–*–SC_{Me}[h]	0.0101	0.0041	0.0009	0.0042	77.3	10.252	127.2	6195
3b: Se–*–SF	0.0498	0.0084	−0.0104	0.0134	141.3	2.704	177.4	21.8
3b: S–*–SeCl	0.0396	0.0080	−0.0057	0.0098	125.3	4.685	168.7	56.0
3b: S–*–SeBr	0.0369	0.0078	−0.0047	0.0091	120.9	5.190	165.0	67.8
3b: S–*–SeI	0.0291	0.0071	−0.0023	0.0074	108.1	6.640	151.7	117
3b: S–*–SeSeMe	0.0163	0.0051	0.0002	0.0051	88.2	8.297	116.7	167
3b: S–*–SeC_{Me}	0.0127	0.0044	0.0006	0.0044	82.4	8.548	105.9	116
4a: Se–*–SF	0.0350	0.0072	−0.004	0.0082	118.8	7.601	163.1	91.7
4a: Se–*–SCl	0.0218	0.0057	−0.0008	0.0057	98.3	9.732	135.3	167
4a: Se–*–SBr	0.0213	0.0056	−0.0007	0.0057	97.5	10.162	134.2	170
4a: Se–*–SI	0.0173	0.0050	−0.0001	0.0050	91.3	12.191	124.8	182
4a: Se–*–SSMe	0.0119	0.0040	0.0005	0.0040	83.2	9.983	112.2	142
4a: Se–*–SC_{Me}	[i]	[i]	[i]	[i]	[i]	[i]	[i]	[i]
4b: Se–*–SeF	0.0470	0.0073	−0.009	0.0116	140.9	2.766	176.7	29.1
4b: Se–*–SeCl	0.0386	0.007	−0.0054	0.0089	127.5	4.565	168.9	62.4
4b: Se–*–SeBr	0.0366	0.0068	−0.0047	0.0083	124.3	4.943	165.8	71.5
4b: Se–*–SeI	0.0296	0.0063	−0.0026	0.0068	112.7	6.399	154.1	115
4b: Se–*–SeSeMe	0.0160	0.0045	−0.0001	0.0045	91.1	8.731	118.5	1154
4b: Se–*–SeC_{Me}	0.0120	0.0038	0.0004	0.0038	84.5	9.347	108.5	47.1
5c: Te–*–TeF	0.0448	0.0033	−0.0115	0.0119	163.8	2.232	184.8	7.5
5c: Te–*–TeCl	0.0402	0.0035	−0.0089	0.0096	158.2	3.087	184.3	15.1
5c: Te–*–TeBr	0.0387	0.0036	−0.0081	0.0089	156.3	3.350	183.9	19
5c: Te–*–TeI	0.0347	0.0037	−0.0062	0.0073	149.3	4.204	182.0	25.1
5c: Te–*–TeTeMe	0.0169	0.0034	−0.0007	0.0035	102.0	8.359	148.7	271
5c: Te–*–TeC_{Me}	0.0136	0.0031	−0.0001	0.0031	92.7	8.869	133.7	335

[a] See text for MP2/BSS-A. [b] $c\nabla^2\rho_b(r_c) = H_b(r_c) - V_b(r_c)/2$, where $c = \hbar^2/8m$. [c] $R = (x^2 + y^2)^{1/2}$, where $(x, y) = (H_b(r_c) - V_b(r_c)/2, H_b(r_c))$. [d] $\theta = 90° - \tan^{-1}(y/x)$. [e] Defined in eqn (3) in the text. [f] $\theta_p = 90° - \tan^{-1}(dy/dx)$. [g] $\kappa_p = |d^2y/dx^2|/[1 + (dy/dx)^2]^{3/2}$. [h] Data from $w = \pm0.0125, \pm0.025, \pm0.050$ being employed for the evaluation. [i] The bond path corresponding to the interaction not detected.

w), while the latter is predicted to have the r-CS/CT-TBP nature. In the case of E = Se, the nature of GSe–*–Y is affected by the change of G and Y. The OSe–*–Cl, OSe–*–Br and OSe–*–I interactions are predicted to have the SS/Cov-w nature with (R, θ, θ_p) of (0.037–0.060 au, 180.4–183.3°, 184.4–191.7°), while NSe–*–Cl, NSe–*–Br and NSe–*–I are predicted to have the r-CS/

 This journal is © The Royal Society of Chemistry 2019

Open Access Article. Published on 29 November 2019. Downloaded on 7/18/2024 8:24:35 PM.
This article is licensed under a Creative Commons Attribution-NonCommercial 3.0 Unported Licence.

Table 2 The nature of the E–*–Y bonds and noncovalent G–*–E interactions in **1a–5c** predicted based on the (R, θ, θ_p) values with MP2/BSS-A[a]

Species: GE–*–Y	R (au)	θ (°)	θ_p (°)	Predicted nature	Species: G–*–EY	θ (°)	θ_p (°)	Predicted nature
1a: NS–*–F	0.1556	183.0	175.2	SS/Cov	**1a**: N–*–SF	162.0	189.9	r-CS/CT-TBP
1a: NS–*–Cl	0.0536	180.5	195.6	SS/Cov-w	**1a**: N–*–SCl	153.4	187.7	r-CS/CT-TBP
1a: NS–*–Br	0.0375	176.7	193.9	r-CS/CT-TBP	**1a**: N–*–SBr	150.2	186.4	r-CS/CT-TBP
1a: NS–*–I	0.0340	180.3	192.8	SS/Cov-w	**1a**: N–*–SI	132.0	179.2	r-CS/CT-MC
1a: NS–*–SMe	0.0936	191.1	197.6	SS/Cov-w	**1a**: N–*–SSMe	84.1	106.0	p-CS/t-HB_{nc}
1a: NS–*–C_{Me}	0.1309	196.0	199.7	SS/Cov-w	**1a**: N–*–SC_{Me}	79.7	96.1	p-CS/t-HB_{nc}
1b: NSe–*–F	0.0830	155.0	146.9	r-CS/t-HB_{wc}	**1b**: N–*–SeF	155.6	182.4	r-CS/CT-TBP
1b: NSe–*–Cl	0.0417	174.7	187.3	r-CS/CT-TBP	**1b**: N–*–SeCl	152.1	183.1	*r* CS/CT-TBP
1b: NSe–*–Br	0.0307	173.3	189.5	r-CS/CT-TBP	**1b**: N–*–SeBr	150.0	182.6	r-CS/CT-TBP
1b: NSe–*–I	0.0260	177.3	191.7	r-CS/CT-TBP	**1b**: N–*–SeI	141.5	180.5	r-CS/CT-TBP
1b: NSe–*–SeMe	0.0485	185.6	194.2	SS/Cov-w	**1b**: N–*–SeSeMe	98.2	140.3	r-CS/t-HB_{wc}
1b: NSe–*–C_{Me}	0.0998	193.0	192.7	SS/Cov-w	**1b**: N–*–SeC_{Me}	85.3	107.5	p-CS/t-HB_{nc}
2a: OS–*–F	0.1964	177.0	136.3	r-CS/t-HB_{wc}	**2a**: O–*–SF	90.3	124.6	r-CS/t-HB_{wc}
2a: OS–*–Cl	0.0890	188.1	196.4	SS/Cov-w	**2a**: O–*–SCl	80.8	95.0	p-CS/t-HB_{nc}
2a: OS–*–Br	0.0611	185.3	195.2	SS/Cov-w	**2a**: O–*–SBr	79.9	92.5	p-CS/t-HB_{nc}
2a: OS–*–I	0.0483	183.9	187.9	SS/Cov-w	**2a**: O–*–SI	78.1	88.2	p-CS/vdW
2a: OS–*–SMe	0.0971	191.4	197.5	SS/Cov-w	**2a**: O–*–SSMe	76.5	84.9	p-CS/vdW
2a: OS–*–C_{Me}	0.1320	196.0	199.7	SS/Cov-w	**2a**: O–*–SC_{Me}	75.7	84.4	p-CS/vdW
2b: OSe–*–F	0.1018	153.7	141.8	r-CS/t-HB_{wc}	**2b**: O–*–SeF	101.4	147.4	r-CS/t-HB_{wc}
2b: OSe–*–Cl	0.0603	180.4	184.4	SS/Cov-w	**2b**: O–*–SeCl	91.1	125.9	r-CS/t-HB_{wc}
2b: OSe–*–Br	0.0448	181.1	190.8	SS/Cov-w	**2b**: O–*–SeBr	88.9	119.2	p-CS/t-HB_{nc}
2b: OSe–*–I	0.0367	183.3	191.7	SS/Cov-w	**2b**: O–*–SeI	84.4	105.3	p-CS/t-HB_{nc}
2b: OSe–*–SeMe	0.0533	186.7	194.0	SS/Cov-w	**2b**: O–*–SeSeMe	79.4	89.0	p-CS/vdW
2b: OSe–*–C_{Me}	0.1016	193.2	192.7	SS/Cov-w	**2b**: O–*–SeC_{Me}	77.6	84.2	p-CS/vdW
3a: SS–*–F	0.1840	180.2	150.0	SS/Cov	**3a**: S–*–SF	121.2	167.1	r-CS/CT-MC
3a: SS–*–Cl	0.0825	187.2	196.8	SS/Cov-w	**3a**: S–*–SCl	95.4	133.8	r-CS/t-HB_{wc}
3a: SS–*–Br	0.0569	184.2	195.5	SS/Cov-w	**3a**: S–*–SBr	93.9	131.4	r-CS/t-HB_{wc}
3a: SS–*–I	0.0461	183.6	188.7	SS/Cov-w	**3a**: S–*–SI	87.9	121.5	p-CS/t-HB_{nc}
3a: SS–*–SMe	0.0949	191.2	197.5	SS/Cov-w	**3a**: S–*–SSMe	81.0	109.4	p-CS/t-HB_{nc}
3a: SS–*–C_{Me}	0.1305	196.0	199.7	SS/Cov-w	**3a**: S–*–SC_{Me}	77.3	127.2	p-CS/t-HB_{nc}
3b: SSe–*–F	0.0888	155.1	145.3	r-CS/t-HB_{wc}	**3b**: S–*–SeF	141.3	177.4	r-CS/CT-MC
3b: SSe–*–Cl	0.0503	178.0	188.0	r-CS/CT-TBP	**3b**: S–*–SeCl	125.3	168.7	r-CS/CT-MC
3b: SSe–*–Br	0.0375	177.7	191.9	r-CS/CT-TBP	**3b**: S–*–SeBr	120.9	165.0	r-CS/CT-MC
3b: SSe–*–I	0.0327	181.4	192.7	SS/Cov-w	**3b**: S–*–SeI	108.1	151.7	r-CS/CT-MC
3b: SSe–*–SeMe	0.0515	186.3	194.0	SS/Cov-w	**3b**: S–*–SeSeMe	88.2	116.7	p-CS/t-HB_{nc}
3b: SSe–*–C_{Me}	0.0994	193.3	193.2	SS/Cov-w	**3b**: S–*–SeC_{Me}	82.4	105.9	p-CS/t-HB_{nc}
4a: SeS–*–F	0.1831	180.4	151.3	SS/Cov	**4a**: Se–*–SF	118.8	163.1	r-CS/CT-MC
4a: SeS–*–Cl	0.0807	186.8	196.9	SS/Cov-w	**4a**: Se–*–SCl	98.3	135.3	r-CS/t-HB_{wc}
4a: SeS–*–Br	0.0554	183.9	195.7	SS/Cov-w	**4a**: Se–*–SBr	97.5	134.2	r-CS/t-HB_{wc}
4a: SeS–*–I	0.0454	183.5	189.0	SS/Cov-w	**4a**: Se–*–SI	91.3	124.8	r-CS/t-HB_{wc}
4a: SeS–*–SMe	0.0944	191.2	197.5	SS/Cov-w	**4a**: Se–*–SSMe	83.2	112.2	p-CS/t-HB_{nc}
4a: SeS–*–C_{Me}[c]	0.1308	195.9	199.7	SS/Cov-w	**4a**: Se–*–SC_{Me}	[b]	[b]	[b]
4b: SeSe–*–F	0.0869	155.4	146.0	r-CS/t-HB_{wc}	**4b**: Se–*–SeF	140.9	176.7	r-CS/CT-MC
4b: SeSe–*–Cl	0.0482	177.4	188.5	r-CS/CT-TBP	**4b**: Se–*–SeCl	127.5	168.9	r-CS/CT-MC
4b: SeSe–*–Br	0.0357	176.7	192.0	r-CS/CT-TBP	**4b**: Se–*–SeBr	124.3	165.8	r-CS/CT-MC
4b: SeSe–*–I	0.0313	180.7	192.9	SS/Cov-w	**4b**: Se–*–SeI	112.7	154.1	r-CS/CT-MC
4b: SeSe–*–SeMe	0.0510	186.2	194.0	SS/Cov-w	**4b**: Se–*–SeSeMe	91.1	118.5	r-CS/t-HB_{wc}
4b: SeSe–*–C_{Me}	0.0993	193.1	193.2	SS/Cov-w	**4b**: Se–*–SeC_{Me}	84.5	108.5	p-CS/t-HB_{nc}
5c: TeTe–*–F	0.0655	121.1	115.8	r-CS/t-HB_{wc}	**5c**: Te–*–TeF	163.8	184.8	r-CS/CT-TBP
5c: TeTe–*–Cl	0.0331	163.6	154.9	r-CS/CT-MC	**5c**: Te–*–TeCl	158.2	184.3	r-CS/CT-TBP
5c: TeTe–*–Br	0.0274	170.7	173.0	r-CS/CT-MC	**5c**: Te–*–TeBr	156.3	183.9	r-CS/CT-TBP
5c: TeTe–*–I	0.0236	178.5	188.3	r-CS/CT-TBP	**5c**: Te–*–TeI	149.3	182.0	r-CS/CT-TBP
5c: TeTe–*–TeMe	0.0332	186.9	190.8	SS/Cov-w	**5c**: Te–*–TeTeMe	102.0	148.7	r-CS/t-HB_{wc}
5c: TeTe–*–C_{Me}	0.0615	180.6	163.8	SS/Cov-w	**5c**: Te–*–TeC_{Me}	92.7	133.7	r-CS/t-HB_{wc}

[a] The (R, θ, θ_p) values are shown for the E–*–Y interactions, while the (θ, θ_p) values for the G–*–E interactions. [b] The bond path corresponding to the interaction not detected. [c] Data from $w = \pm0.0125$, ±0.025 and ±0.050 being employed for the evaluation.

CT-TBP nature with (R, θ, θ_p) of (0.026–0.042 au, 173.3–177.3°, 187.3–191.7°). The Se–*–Cl and Se–*–Br interactions with G = S and Se are predicted to have the r-CS/CT-TBP nature with (R, θ, θ_p) of (0.036–0.050 au, 176.7–178.0°, 188.0–192.0°), whereas the SS/Cov-w nature is predicted for Se–*–I, Se–*–SeMe and Se–*–C_{Me} with G = S and Se, as (R, θ, θ_p) are (0.031–0.099 au, 180.7–193.3°, 192.7–194.0°).

Open Access Article. Published on 29 November 2019. Downloaded on 7/18/2024 8:24:35 PM.
This article is licensed under a Creative Commons Attribution-NonCommercial 3.0 Unported Licence.

In the case of Y = F in GE–*–Y, the E–*–F interactions show a specific and complex nature due to the highly electronegative character of F. The (R, θ, θ_p) values are (0.156–0.184 au, 180.2–183.0°, 150.0–175.2°) for GS–*–F with G = N, S and Se. As a result, the bonds could be characterized as Cov-s based on the values of R and θ; however, the θ_p values do not satisfy the requirements for Cov-s (or Cov). Therefore, they are characterized as "Cov" in this work, where θ is superior to θ_p, in this case. The (R, θ, θ_p) values are (0.196 au, 177.0°, 136.3°) for S–*–F with G = O, which is classified as r-CS and characterized as t-HB_{wc} (r-CS/t-HB_{wc}), irrespective of the R value. The observed results must be the reflection of the specific and complex nature of S–*–F, where the R values are much larger than those expected based on the (θ, θ_p) values. The R values of S–*–F are about two times larger than those corresponding S–*–Cl, respectively, although the (θ, θ_p) values for S–*–F are (much) smaller than those corresponding S–*–Cl, respectively. For the Se–*–F interactions, the (R, θ, θ_p) values are (0.083–0.102 au, 153.7–155.4°, 141.8–146.9°) for G = N, O, S and Se; therefore, the interactions are predicted to have the r-CS/t-HB_{wc} nature. The nature of r-CS/t-HB_{wc} predicted for the Se–*–F interactions seems rather curious, which may come from the QTAIM-DFA parameters of $\theta > \theta_p$, although the values are $\theta < \theta_p$ for the usual interactions. The (R, θ, θ_p) values for Te–*–F with G = Te are (0.066 au, 121.1°, 115.8°), which is also predicted to have the r-CS/t-HB_{wc} nature. The R values of Se–*–F are also about two times larger than those corresponding Se–*–Cl, respectively, although the (θ, θ_p) values for Se–*–F are (much) smaller than those corresponding Se–*–Cl.

The nature of the G–*–E interactions of GEY σ(3c–4e) in **1–5** is discussed next. BP with BCP was detected for all G–*–E interactions of **1–5**, except for **4a** (Y = C_{Me}). The Se–*–SC_{Me} interaction in **4a** (Y = C_{Me}) would not satisfy the conditions for the appearance of BP with BCP.[43] Therefore, the nature of the G–*–E interactions in **1–5** is discussed without considering the interaction in **4a** (Y = C_{Me}). The R values in Table 1 are less than 0.031 au, therefore, the nature of the G–*–E interactions in **1–5** can be discussed using the (θ, θ_p) values, except for that of **4a** (Y = C_{Me}). The θ values for G–*–E in **1–5** are in the range of $75.7° \leq \theta \leq 163.8°$; therefore, the G–*–E interactions in **1–5** are classified as p-CS or r-CS interactions.

The nature is discussed on an individual basis. The (θ, θ_p) values for N–*–SY (**1a**: Y = F, Cl and Br), N–*–SeY (**1b**: Y = F, Cl, Br and I) and Te–*–TeY (**5c**: Y = F, Cl, Br and I) are (141.5–163.8°, 180.5–189.9°). Therefore, the interactions are predicted to have the r-CS/CT-TBP nature. The r-CS/CT-MC nature is similarly predicted for N–*–SY (**1a**: Y = I), S–*–SY (**3a**: Y = F), S–*–SeY (**3b**: Y = F, Cl, Br and I), Se–*–SY (**4a**: Y = F) and Se–*–SeY (**4b**) (Y = F, Cl, Br and I), as the (θ, θ_p) values are (108.1–141.3°, 151.7–179.2°). Alternatively, the p-CS/vdW nature is predicted for O–*–SY (**2a**: Y = I, SMe and Me) and O–*–SeY (**2b**: Y = SeMe and Me) with (θ, θ_p) = (75.7–79.4°, 84.2–89.0°), while the p-CS/t-HB_{nc} nature is predicted for N–*–SY (**1a**: Y = SMe and Me), N–*–SeY (**1b**: Y = Me), O–*–SY (**2a**: Y = Cl and Br), O–*–SeY (**2b**: Y = Br and I), S–*–SY (**3a**: Y = I, SMe and Me), S–*–SeY (**3b**: Y = SeMe and Me), Se–*–SY (**4a**: Y = SMe) and Se–*–SeY (**4b**: Y = Me) with (θ, θ_p) = (77.3–88.9°, 92.5–127.2°). The (θ, θ_p) values are (90.3–102.0°, 118.5–148.7°) for N–*–SeY (**1b**: Y = SeMe), O–*–SeY (**2a**: Y = F), O–*–SeY (**2b**: Y = F and Cl), S–*–SY (**3a**: Y = Cl and Br), Se–*–SY (**4a**: Y = Cl, Br and I), Se–*–SeY (**4b**: Y = SeMe) and Te–*–TeY (**5c**: Y = TeMe and Me); therefore, the p-CS/t-HB_{wc} nature is predicted for the interactions.

The values of ($H_b(r_c) - V_b(r_c)/2$, $H_b(r_c)$) for O–*–SeCl (**2b**) and O–*–SeBr (**2b**) are (0.0126 au, −0.0003 au) and (0.0119 au, 0.0002 au), respectively, as shown in Table 1, although the values have been reported as (0.0106 au, −0.0013 au) and (0.0099 au, −0.0011 au), respectively.[13c] The $H_b(r_c) - V_b(r_c)/2$ values for O–*–SeCl (**2b**) and O–*–SeBr (**2b**) in literature are approximately 0.002 au smaller than those in Table 1, while the $H_b(r_c)$ values in the literature are more than 0.001 au smaller than those in Table 1. The differences seem small, however, the values are just on the borderline between the t-HB_{nc} and t-HB_{wc} natures. Specifically, the positive values of $H_b(r_c)$ correspond to the pure CS nature with no covalency (p-CS/t-HB_{nc}), whereas the negative values represent the regular CS nature with covalency (r-CS/t-HB_{wc}). Therefore, it is necessary to select the basis sets and levels for the calculations very carefully.[33] We believe that MP2/6-311+(3df, 3pd) or greater methods, such as MP2/BSS-A, would be necessary if the results are discussed in relation to the observed structural parameters.

The predicted nature for G–*–EY in **1a–5c** is summarized in Fig. 4. The strength of the G–*–E interactions seems weakest for O–*–S and becomes stronger in the order shown in eqn (9). As shown in Fig. 4, the E–Y bonds in **1a–5c** affect the strength of the G–*–E interaction. The effect seems smallest for C_{Me} and becomes larger in the order shown in eqn (10).

$$\text{G–*–EY} = \text{O–*–SY} < \text{O–*–SeY} < \text{S–*–SY} < \text{Se–*–SY} < \text{S–*–SeY} < \text{Se–*–SeY} < \text{N–*–SY} < \text{N–*–SeY} \approx \text{Te–*–TeY} \quad (9)$$

$$\text{GE–*–Y} = \text{GE–*–C}_{\text{Me}} < \text{GE–*–EMe} < \text{GE–*–I} < \text{GE–*–Br} < \text{GE–*–Cl} < \text{GE–*–F} \quad (10)$$

The strength of G–*–EY in GEY σ(3c–4e) of **1a–5c** can also be evaluated by the NBO analysis, where donor NBO and acceptor NBO must be related to n(G) and σ*(E–Y), respectively. The results are discussed in relation to those of the NBO analysis.

NBO analysis for G–*–EY in GEY σ(3c–4e) of 1a–5c

The stabilization energy $E(2)$ in NBO analysis[44] is calculated for each donor NBO(i) and acceptor NBO(j) based on the second-order perturbation theory according to eqn (11). The q_i value in eqn (11) is the donor orbital occupancy, E_i, E_j are diagonal elements (orbital energies) and $F(i,j)$ is the off-diagonal NBO Fock matrix element. The treatments evaluate the CT terms of the intramolecular interactions.

$$E(2) = q_i F(i,j)^2/(E_j - E_i) \quad (11)$$

NBO is applied to **1a–5c** (see, Scheme 1d for the simplified interaction model of G–*–EY in GEY σ(3c–4e)). The $E(2)$ values were successfully obtained under the threshold of 0.5 kcal mol^{-1} (2.1 kJ mol^{-1}). The results of NBO analysis,

Open Access Article. Published on 29 November 2019. Downloaded on 7/18/2024 8:24:35 PM.
This article is licensed under a Creative Commons Attribution-NonCommercial 3.0 Unported Licence.

G-*-EY (No)	Y = F	Cl	Br	I	EMe	C_{Me}
Te-*-TeY (**5c**)	TBP	TBP	TBP	TBP	*t*-HBwc	*t*-HBwc
N-*-SeY (**1b**)	TBP	TBP	TBP	TBP	*t*-HBwc	*t*-HBnc
N-*-SY (**1a**)	TBP	TBP	TBP	MC	*t*-HBnc	*t*-HBnc
Se-*-SeY (**4b**)	MC	MC	MC	MC	*t*-HBwc	*t*-HBnc
S-*-SeY (**3b**)	MC	MC	MC	MC	*t*-HBnc	*t*-HBnc
Se-*-SY (**4a**)	MC	*t*-HBwc	*t*-HBwc	*t*-HBwc	*t*-HBnc	nd
S-*-SY (**3a**)	MC	*t*-HBwc	*t*-HBwc	*t*-HBnc	*t*-HBnc	*t*-HBnc
O-*-SeY (**2b**)	*t*-HBwc	*t*-HBwc	*t*-HBnc	*t*-HBnc	vdW	vdW
O-*-SY (**2a**)	*t*-HBwc	*t*-HBnc	*t*-HBnc	vdW	vdW	vdW

Fig. 4 The nature of the G–*–EY interactions in GEY σ(3c–4e) of **1a–5c** predicted with MP2/BSS-A. The interaction nature of CT-TBP, CT-MC and vdW shows that of the trigonal bipyramidal adduct formation through CT, molecular complex formation through CT and van der Waals interaction, respectively, while t-HB_{wc} and t-HB_{nc} do the typical hydrogen bonds with and without the covalency, respectively, and nd means not detected.

calculated with MP2/BSS-A, are shown in Table S5 of the ESI.† No data were detected for the $n_p(N) \rightarrow \sigma^*(E–Y)$ interactions in **1a** and **1b**, as the only one nonbonded orbital of N is characterized as s-type ($n_s(N)$) (see Table S5 of the ESI†). In the case of **1a**, **1b**, **2b**, **3a**, **3b**, **4b** and **5c**, the E–F bonds (E = S, Se and Te) are described as the ionic $E^+–F^-$ bonds in the NBO framework, since the valence orbitals of F are almost fully filled with electrons. The orbitals for the ionic $E^+–F^-$ bonds are described as $n_p(E^+$: E = S, Se and Te) and $n_p(F^-)$ in Table S5 of the ESI.† Instead, the S–F bonds in **2a** and **4a** are denoted as S–F bonds. Very large values of $E(2)$ were predicted for $n_s(N) \rightarrow n_p(E^+$: E = S and Se) in **1a** and **1b** and $n_p(E) \rightarrow n_p(E^+)$ for (E, E^+) = (O, Se^+) in **2a**, (S, S^+) in **3a**, (S, Se^+) in **3b**, (Se, Se^+) in **4b** and (Te, Te^+) in **5c**. The $E(2)$ values are larger than 20 kcal mol^{-1} and up to 126 kcal mol^{-1} in **5c**. Very large values of $E(2)$ were also predicted for $n_s(N) \rightarrow \sigma^*(S–Y)$ in **1a**, $n_s(N) \rightarrow \sigma^*(Se–Y)$ in **1b**, $n_p(S) \rightarrow \sigma^*(Se–Y)$ in **3b**, $n_p(Se) \rightarrow \sigma^*(Se–Y)$ in **4b** and $n_p(Te) \rightarrow \sigma^*(Te–Y)$ in **5c**, where Y = Cl, Br and/or I. As shown in Table S5 of the ESI,† the predicted $E(2)$ values for G–*–EY in **1a–5c** will be stronger in an order similar to that shown in eqn (9). The order for $E(2)$ evaluated with NBO shown in eqn (12) is in accordance with that estimated with QTAIM-DFA shown in eqn (9).

$$G–*–EY = O–*–SY \ll O–*–SeY \approx S–*–SY \approx Se–*–SY \ll S–*–SeY < Se–*–SeY < N–*–SY < N–*–SeY \ll Te–*–TeY \quad (12)$$

The $E(2)$ values are also larger than 20 kcal mol^{-1}, and this value is greater than 60 kcal mol^{-1} in **5c**. The $E(2)$ values for $n_p(G) \rightarrow \sigma^*(E–Y)$, other than those given above, are less than 12 kcal mol^{-1}, while those for $n_s(E) \rightarrow n_p(E'^+)$ and $n_s(G) \rightarrow \sigma^*(E–Y)$ in **2a–5c** are less than approximately 5 kcal mol^{-1}. Some $E(2)$ values were not detected for $n_s(G) \rightarrow \sigma^*(E–Y)$, which would be smaller than the threshold values of 0.5 kcal mol^{-1} (see Table S5 of the ESI†).

It is noteworthy that the $E(2)$ values for $n_s(N) \rightarrow n_p(E^+$: E = S and Se) in **1a** and **1b** and the combined values of $n_s(G) \rightarrow \sigma^*(E–Y)$ and $n_p(G) \rightarrow \sigma^*(E–Y)$ seem to increase proportionally to the inverse values of C_{ii}, the diagonal elements of the compliance constants for an internal coordinate i, (C_{ii}^{-1}). To confirm the proportionality, the $E(2)$ values are plotted *versus* C_{ii}^{-1}, separately by **1a**, **1b**, **2** (**2a** and **2b**) and **3–5** (**3a**, **3b**, **4a**, **4b** and **5c**). Fig. 5 shows the plot and the correlations are very good. The correlation for **3–5** ($y = -24.68 + 317.6x$: $R_c^2 = 0.933$) will be better if the data point of **3a** (S–*–SF) is omitted from the correlation ($y = -26.49 + 322.1x$: $R_c^2 = 0.961$). As also shown in Fig. 5, the tangent lines for the correlations (a in $y = ax + b$) become larger in the order of **2** ($a = 88$) < **1a** (113) ≈ **1b** (122) ≪ **3–5** (318). It is noteworthy that the CT contributions in G–*–EY of GEY σ(3c–4e) in **1a–5c** can also be estimated based of the C_{ii} (or C_{ii}^{-1}) values. Very good proportionality will be observed if the $E(2)$ values are plotted *versus* C_{ii}^{-1} and are analysed suitably separated by G.

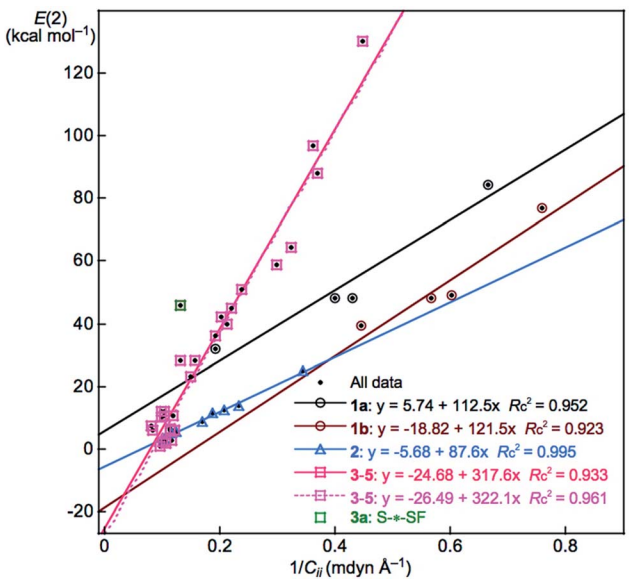

Fig. 5 Plots of $E(2)$ *versus* C_{ii}^{-1}, separately by **1a**, **1b**, **2** and **3–5**, calculated with MP2/BSS-A. A better correlation shown by the pink dotted line was obtained when data corresponding to that for **3a** (S–*–SF) was neglected.

Open Access Article. Published on 29 November 2019. Downloaded on 7/18/2024 8:24:35 PM.
This article is licensed under a Creative Commons Attribution-NonCommercial 3.0 Unported Licence.

Conclusions

Weak interactions in chemistry determine the fine details of structures and create fine properties in materials, while strong interactions construct the framework of molecules. Three centre four electron interactions of the σ-type (σ(3c–4e)) are typical cases of such weak interactions. The noncovalent G···E interactions and the (covalent) E–Y bonds in GEY σ(3c–4e) of *o*-$Me_nGCH_2C_6H_4EY$ are elucidated with the QTAIM dual functional analysis (QTAIM-DFA) and QC calculations. The system detects delicate interactions by considering the suitable rigidity. The dynamic nature of the interactions can be discussed by applying QTAIM-DFA in addition to the static nature. The dynamic nature is called the intrinsic dynamic nature if the perturbed structures are generated using the coordinates derived from the compliance constants in QTAIM-DFA, as the coordinates are invariant to the choice of coordinate system. The E–*–Y bonds are typically classified as the SS interactions for G = N, O, S and Se, although there are some exceptions. The E–F bonds are described as ionic E^+–F^- bonds for all GE–F, except for OS–F (**2a**), in the NBO framework. In the case of the noncovalent G–*–E interactions of GEY σ(3c–4e), these interactions are predicted to have vdW to CT-TBP natures. The strength of G–*–E seems weakest for O–*–S and becomes stronger in the order show in eqn (9). The G–*–E interactions apparently inversely affect the strength of the E–Y bonds.

The strength of G–*–EY in GEY σ(3c–4e) is also evaluated with NBO. Very large values of $E(2)$ were predicted for $n_s(N) \rightarrow n_p(E^+$: E = S and Se) and $n_p(E) \rightarrow n_p(E^+)$ for (E, E^+) = (O, Se^+), (S, S^+), (S, Se^+), (Se, Se^+) and (Te, Te^+) ($Y^- = F^-$). The $E(2)$ value results in 126 kcal mol^{-1} in **5c**. The predicted $E(2)$ values for G–*–EY in **1a–5c** will be stronger in the similar order shown in eqn (12). The order for $E(2)$ determined with NBO seems to be in accordance with that estimated with the QTAIM approach. It is noteworthy that $E(2)$ increases in a manner inversely proportional to C_{ii} (C_{ii}^{-1}). The proportionality is demonstrated by the plot of $E(2)$ *versus* C_{ii}^{-1}. The results show that the contributions from the CT interactions in G–*–EY of **1a–5c** can be estimated by the C_{ii} (C_{ii}^{-1}) values. Very good proportionality will be observed if the $E(2)$ values are plotted *versus* C_{ii}^{-1} and are analysed suitably separated by G (and E). As a result, C_{ii} (or C_{ii}^{-1}) will be a good tool to elucidate the complex energy profiles of species.

Conflicts of interest

The authors declare no conflict of interest.

Acknowledgements

This work was partially supported by a Grant-in-Aid for Scientific Research (No. 17K05785) from the Ministry of Education, Culture, Sports, Science and Technology, Japan. L. S. acknowledges the European Union's Horizon 2020 research and innovation programme under the Marie Skłodowska-Curie grant agreement No 665778 – POLONEZ funding programme, National Science Centre, Poland – project registration number 2016/21/P/ST5/03512. This work was performed under the umbrella of the network Selenium Sulfur and Redox Catalysis (SeSRedCat).

Notes and references

1 A. J. Pacuła, F. Mangiavacchi, L. Sancineto, J. L. Eder, J. Ścianowski and C. Santi, *Curr. Chem. Biol.*, 2015, **9**, 97–112.
2 (*a*) G. C. Pimentel, *J. Chem. Phys.*, 1951, **19**, 446–448; (*b*) J. I. Musher, *Angew. Chem., Int. Ed. Engl.*, 1969, **8**, 54–68; (*c*) R. J. Hatch and R. E. Rundle, *J. Am. Chem. Soc.*, 1951, **73**, 4321–4324; (*d*) R. E. Rundle, *J. Am. Chem. Soc.*, 1963, **85**, 112–113; (*e*) R. A. Hayes and J. C. Martin, *Sulfurane Chemistry in Organic Sulfur Chemistry: Theoretical and Experimental Advances*, ed. F. Bernardi, I. G. Csizmadia and A. Mangini, Elsevier, Amsterdam, 1985; ch. 8.
3 (*a*) M. M. L. Chen and R. J. Hoffmann, *J. Am. Chem. Soc.*, 1976, **98**, 1647–1653; (*b*) P. J. Hay, *J. Am. Chem. Soc.*, 1977, **99**, 1003–1012; (*c*) W. Kutzelnigg, *Angew. Chem., Int. Ed. Engl.*, 1984, **23**, 272–295; (*d*) A. E. Reed and F. Weinhold, *J. Am. Chem. Soc.*, 1986, **108**, 3586–3593; (*e*) A. E Reed and P. R. Schleyer, *J. Am. Chem. Soc.*, 1990, **112**, 1434–1445.
4 (*a*) *Chemistry of Hypervalent Compounds*, ed. K.-y. Akiba, Wiley-VCH, New York, 1999; (*b*) W. Nakanishi, *Hypervalent Chalcogen Compounds In Handbook of Chalcogen Chemistry: New Perspectives in Sulfur, Selenium and Tellurium*, ed. F. A. Devillanova, Royal Society of Chemistry, Cambridge, 2006, ch. 10.3, pp. 644–668; (*c*) A. J. Mukherjee, S. S. Zade, H. B. Singh and R. B. Sunoj, *Chem. Rev.*, 2010, **110**, 4357–4416.
5 G. Buemi, Intramolecular Hydrogen Bonds. Methodologies and Strategies for Their Strength Evaluation, in *Hydrogen Bonding – New Insights, Vol. 3, Challenges and Advances in Computational Chemistry and Physics*, ed. S. J. Grabowski, Springer, New York, 2006, ch. 2.
6 G. Gilli and P. Gilli, *The Nature of the Hydrogen Bond: Outline of a Comprehensive Hydrogen Bond Theory (IUCr Monographs on Crystallography)*, Oxford University Press, Oxford, 2009.
7 M. Meot-Ner (Mautner), *Chem. Rev.*, 2005, **105**, 213–284.
8 G. Cavallo, P. Metrangolo, R. Milani, T. Pilati, A. Priimagi, G. Resnati and G. Terraneo, *Chem. Rev.*, 2016, **116**, 2478–2601.
9 S. Hayashi, K. Matsuiwa, M. Kitamoto and W. Nakanishi, *J. Phys. Chem. A*, 2013, **117**, 1804–1816.
10 T. Nishide, S. Hayashi and W. Nakanishi, *ChemistryOpen*, 2018, **7**, 565–575.
11 (*a*) W. Nakanishi, S. Hayashi, A. Sakaue, G. Ono and Y. Kawada, *J. Am. Chem. Soc.*, 1998, **120**, 3635–3640; (*b*) W. Nakanishi, S. Hayashi and T. Uehara, *J. Phys. Chem. A*, 1999, **103**, 9906–9912; (*c*) W. Nakanishi and S. Hayashi, *J. Org. Chem.*, 2002, **67**, 38–48; (*d*) K. Yamane, S. Hayashi, W. Nakanishi, T. Sasamori and N. Tokitoh, *Polyhedron*, 2008, **27**, 3557–3566; (*e*) S. Hayashi and W. Nakanishi, *Bull. Chem. Soc. Jpn.*, 2008, **81**, 1605–1615; (*f*) S. Hayashi and W. Nakanishi, *Bull. Chem. Soc. Jpn.*, 2009, **82**, 712–722; (*g*) T. Nakai, M. Nishino, S. Hayashi, M. Hashimoto and W. Nakanishi, *Dalton Trans.*, 2012, **41**, 7485–7497; (*h*)

 This journal is © The Royal Society of Chemistry 2019

Open Access Article. Published on 29 November 2019. Downloaded on 7/18/2024 8:24:35 PM.
This article is licensed under a Creative Commons Attribution-NonCommercial 3.0 Unported Licence.

S. Hayashi, M. Uegaito, T. Nishide, E. Tanaka, W. Nakanishi, T. Sasamori, N. Tokitoh and M. Minoura, *New J. Chem.*, 2019, **43**, 14224–14237.

12 M. Tiecco, L. Testaferri, C. Santi, C. Tomassini, S. Santoro, F. Marini, L. Bagnoli, A. Temperini and F. Costantino, *Eur. J. Org. Chem.*, 2006, 4867–4873.

13 (*a*) M. Iwaoka and S. Tomoda, *J. Am. Chem. Soc.*, 1996, **118**, 8077–8084; (*b*) M. Iwaoka, H. Komatsu, T. Katsuda and S. Tomoda, *J. Am. Chem. Soc.*, 2002, **124**, 1902–1909; (*c*) M. Iwaoka, H. Komatsu, T. Katsuda and S. Tomoda, *J. Am. Chem. Soc.*, 2004, **126**, 5309–5317; (*d*) M. Iwaoka, T. Katsuda, H. Komatsu and S. Tomoda, *J. Org. Chem.*, 2005, **70**, 321–327.

14 E. Espinosa, I. Alkorta, J. Elguero and E. Molins, *J. Chem. Phys.*, 2002, **117**, 5529See also R. Bianchi, G. Gervasio and D. Marabello, *C. R. Chim.*, 2005, **8**, 1392.

15 The natures of G–*–E in **I** with various (G, E–Y) were also elucidated.[11h,45,46]

16 *Atoms in Molecules. A Quantum Theory*, ed. R. F. W. Bader, Oxford University Press, Oxford, UK, 1990.

17 C. F. Matta and R. J. Boyd, in *An Introduction to the Quantum Theory of Atoms in Molecules In The Quantum Theory of Atoms in Molecules: From Solid State to DNA and Drug Design*, ed. C. F. Matta and R. J. Boyd, Wiley-VCH, Weinheim, Germany, 2007, ch. 1.

18 (*a*) R. F. W. Bader, T. S. Slee, D. Cremer and E. Kraka, *J. Am. Chem. Soc.*, 1983, **105**, 5061; (*b*) R. F. W. Bader, *Chem. Rev.*, 1991, **91**, 893; (*c*) R. F. W. Bader, *J. Phys. Chem. A*, 1998, **102**, 7314; (*d*) F. Biegler-könig, R. F. W. Bader and T. H. Tang, *J. Comput. Chem.*, 1982, **3**, 317; (*e*) R. F. W. Bader, *Acc. Chem. Res.*, 1985, **18**, 9; (*f*) T. H. Tang, R. F. W. Bader and P. MacDougall, *Inorg. Chem.*, 1985, **24**, 2047; (*g*) F. Biegler-König, J. Schönbohm and D. Bayles, *J. Comput. Chem.*, 2001, **22**, 545; (*h*) F. Biegler-König and J. Schönbohm, *J. Comput. Chem.*, 2002, **23**, 1489.

19 J. A. Dobado, H. Martínez-García and M. R. Sundberg, *J. Am. Chem. Soc.*, 2000, **122**, 1144.

20 J. M. Molina and J. A. Dobado, *Theor. Chem. Acc.*, 2001, **105**, 328.

21 S. K. Ignatov, N. H. Rees, B. R. Tyrrell, S. R. Dubberley, A. G. Razuvaev, P. Mountford and G. I. Nikonov, *Chem.–Eur. J.*, 2004, **10**, 4991.

22 W. Nakanishi, T. Nakamoto, S. Hayashi, T. Sasamori and N. Tokitoh, *Chem.–Eur. J.*, 2007, **13**, 255.

23 Dots are usually employed to show BCPs in molecular graphs. Therefore, A–•–B would be more suitable to describe the BP with the BCP. Nevertheless, A–*–B is employed to emphasize the existence of the BCP on the BP, in question, in our case.

24 (*a*) W. Nakanishi, S. Hayashi and K. Narahara, *J. Phys. Chem. A*, 2009, **113**, 10050–10057; (*b*) W. Nakanishi, S. Hayashi and K. Narahara, *J. Phys. Chem. A*, 2008, **112**, 13593–13599.

25 W. Nakanishi and S. Hayashi, *Curr. Org. Chem.*, 2010, **14**, 181–197.

26 W. Nakanishi and S. Hayashi, *J. Phys. Chem. A*, 2010, **114**, 7423–7430.

27 W. Nakanishi, S. Hayashi, K. Matsuiwa and M. Kitamoto, *Bull. Chem. Soc. Jpn.*, 2012, **85**, 1293–1305.

28 W. Nakanishi and S. Hayashi, *J. Phys. Chem. A*, 2013, **117**, 1795–1803.

29 QTAIM-DFA parameters of (R, θ) and (θ_p, κ_p) are defined as: $R = (x^2 + y^2)^{1/2}$, where $(x,y) = (H_b(r_c) - V_b(r_c)/2, H_b(r_c))$, $\theta = 90^\circ - \tan^{-1}(y/x)$, $\theta_p = 90^\circ - \tan^{-1}(dy/dx)$, and $\kappa_p = |d^2y/dx^2|/[1 + (dy/dx)^2]^{3/2}$. (See, eqn. (S3)–(S6) of the ESI.†).

30 W. Nakanishi and S. Hayashi, *Int. J. Quantum Chem.*, 2018, **118**, e25590.

31 The C_{ii} values and the coordinates corresponding to C_{ii} were calculated by using the Compliance 3.0.2 program released by Grunenberg and Brandhorst, http://www.oc.tu-bs.de/Grunenberg/compliance.html.

32 (*a*) K. Brandhorst and J. Grunenberg, *J. Chem. Phys.*, 2010, **132**, 184101–184107; (*b*) K. Brandhorst and J. Grunenberg, *Chem. Soc. Rev.*, 2008, **37**, 1558–1567; (*c*) J. Grunenberg, *Chem. Sci.*, 2015, **6**, 4086–4088.

33 S. Hayashi, T. Nishide, K. Ueda, K. Hayama and W. Nakanishi, *ChemistrySelect*, 2019, **4**, 6198–6208.

34 M. J. Frisch, G. W. Trucks, H. B. Schlegel, G. E. Scuseria, M. A. Robb, J. R. Cheeseman, G. Scalmani, V. Barone, B. Mennucci, G. A. Petersson, H. Nakatsuji, M. Caricato, X. Li, H. P. Hratchian, A. F. Izmaylov, J. Bloino, G. Zheng, J. L. Sonnenberg, M. Hada, M. Ehara, K. Toyota, R. Fukuda, J. Hasegawa, M. Ishida, T. Nakajima, Y. Honda, O. Kitao, H. Nakai, T. Vreven, J. A. Montgomery Jr., J. E. Peralta, F. Ogliaro, M. Bearpark, J. J. Heyd, E. Brothers, K. N. Kudin, V. N. Staroverov, R. Kobayashi, J. Normand, K. Raghavachari, A. Rendell, J. C. Burant, S. S. Iyengar, J. Tomasi, M. Cossi, N. Rega, J. M. Millam, M. Klene, J. E. Knox, J. B. Cross, V. Bakken, C. Adamo, J. Jaramillo, R. Gomperts, R. E. Stratmann, O. Yazyev, A. J. Austin, R. Cammi, C. Pomelli, J. W. Ochterski, R. L. Martin, K. Morokuma, V. G. Zakrzewski, G. A. Voth, P. Salvador, J. J. Dannenberg, S. Dapprich, A. D. Daniels,Ö. Farkas, J. B. Foresman, J. V. Ortiz, J. Cioslowski and D. J. Fox, *Gaussian 09, Revision D.01*, Gaussian, Inc., Wallingford CT, 2009.

35 E. D. Glendening, C. R. Landis and F. Weinhold, NBO 6.0: Natural bond orbital analysis program, *J. Comput. Chem.*, 2013, **34**, 1429–1437.

36 T. Noro, M. Sekiya and T. Koga, *Theor. Chem. Acc.*, 2012, **131**, 1124.

37 (*a*) C. Møller and M. S. Plesset, *Phys. Rev.*, 1934, **46**, 618–622; (*b*) J. Gauss, *J. Chem. Phys.*, 1993, **99**, 3629–3643; (*c*) J. Gauss, *Ber. Bunsen-Ges. Phys. Chem.*, 1995, **99**, 1001–1008.

38 The perturbed structures with CIV correspond to the improved ones of the vibrational mode for each zero-point internal vibration. Therefore, each perturbed structure with CIV can be imaged based on the vibrational mode of the zero-point internal vibration. The perturbed structures with CIV are very close to those obtained with POM, so are the relative energies.

39 The AIM2000 program (Version 2.0) is employed to analyze and visualize atoms-in-molecules: F. Biegler-König, *J. Comput. Chem.*, 2000, **21**, 1040–1048. See also ref. 16.

Open Access Article. Published on 29 November 2019. Downloaded on 7/18/2024 8:24:35 PM.
This article is licensed under a Creative Commons Attribution-NonCommercial 3.0 Unported Licence.

40 T. A. Keith, *AIMAll (Version 17.11.14), TK Gristmill Software*, Overland Park KS, USA, 2017, aim.tkgristmill.com.

41 E. Espinosa and coworkers discussed the behaviour of the interactions in the wide view based on the QTAIM functions at BCPs on H···F of the fully optimized various X–H···F–Y and those on the partially optimized $[F–H–F]^-$.[14] On the other hand, we employed the standard interactions in the typical species and the wide range of perturbed structures of $[Cl–Cl–Cl]^-$ for the purpose. QTAIM-DFA parameters, instead of the QTAIM functions, are employed for the classification and characterization of interactions, after treatment of Q TAIM-DFA.[24a,30]

42 The (R, θ, θ_p:CIV) values are evaluated to be (0.354 au, 180.3°, 154.5°), (0.152 au, 194.4°, 198.4°), and (0.102 au, 192.8°, 195.9°) for the C–*–F, C–*–Cl, and C–*–Cl bonds, respectively, in CH_3X (X = F, Cl and Br) of which R value of C–*–F is predicted to be very large. See also the ESI of ref. 27 for the QTAIM parameters of the fluorine containing interactions.

43 The bond path corresponding to the interaction being not detected.

44 E. D. Glendening, A. E. Reed, J. E. Carpenter and F. Weinhold, *NBO 3.0 Program Manual*, Theoretical Chemistry Institute, University of Wisconsin, Madison, WI, USA, 1990.

45 The (θ, θ_p) values are determined for (G, EY) = (MeO, SMe), (MeO, SeMe), (MeS, SeMe), (MeS, SMe), (MeSe, SeMe) and (MeTe, TeMe) in **I** to be (83.4, 96.0), (85.1, 101.2), (100.9, 133.4), (98.0, 126.2), (101.2, 130.5), and (122.3, 165.8), respectively. The (θ, θ_p) values for **I** are larger than the corresponding values in **2–5**, respectively.[11h,46]

46 The (θ and θ_p) values of **I** were plotted *versus* the corresponding values of **2–5**, which gave a very good correlation ($y = 1.36x - 13.89$: $R_c^2 = 0.954$, although the data for (MeS, SMe) being omitted from the correlation). The plot is shown in Fig. S6 of the ESI.†

This journal is © The Royal Society of Chemistry 2019